Catalytic Porous Ceramic Prepared In-Situ by Sol-Gelation for Butane-to-Syngas Processing in Microreactors

Nico Hotz, Nurten Koc, Timo Schwamb, Niklas C. Schirmer, and Dimos Poulikakos
Dept. of Mechanical and Process Engineering, Laboratory of Thermodynamics in Emerging Technologies, Institute of Energy Technology, ETH Zurich, CH-8092 Zurich, Switzerland

DOI 10.1002/aic.11831
Published online May 18, 2009 in Wiley InterScience (www.interscience.wiley.com).

In this study, a novel flow-based method is presented to place catalytic nanoparticles into a reactor by sol-gelation of a porous ceramic consisting of Rh/ceria/zirconia nanoparticles, silica sand, ceramic binder, and a gelation agent. This method allows for the placement of a liquid precursor containing the catalyst into the final reactor geometry without the need of impregnating or coating of a substrate with the catalytic material. The so generated foam-like porous ceramic shows properties highly appropriate for use as catalytic reactor material, e.g., reasonable pressure drop due to its porosity, high thermal and catalytic stability, and excellent catalytic behavior. To investigate the catalytic activity, microreactors containing this foam-like ceramic are employed for the production of hydrogen and carbon monoxide-rich syngas from butane. The effect of operating parameters such as the inlet flow rate on the hydrocarbon processing is analyzed and the limitation of the reactor by diffusion mass transport is investigated. © 2009 American Institute of Chemical Engineers *AIChE J,* 55: 1849–1859, 2009
Keywords: catalytic porous ceramic, butane-to-syngas processing, catalytic foam, sol-gelation, Rh catalyst

Introduction

Ceramic foams or sponges are seen as a very promising material for structured catalyst supports due to their porosity, open-cell structure, thermal and chemical stability, and variable thermal conductivity depending on the support material. The typical fabrication procedure of such a catalytic foam is to first generate a porous ceramic as support and then coat this foam in a second step with the catalyst using different coating methods.[1] A very common method is the impregnation of the calcined ceramic foam with a liquid precursor containing the catalyst.[2–4] An interesting idea is to fabricate the ceramic foam support by sol-gelation[3] or to use a sol-gelation method to apply the catalyst on the ceramic foam support.[5]

Correspondence concerning this article should be addressed to D. Poulikakos at dimos.poulikakos@ethz.ch.

The novelty of the herein presented method is to fabricate a foam-like porous ceramic containing a catalyst in form of nanoparticles in a direct one-step method by sol-gelation avoiding any separate coating or impregnation step.[6] Reitzmann et al.[2] claimed that a one-step method is usually not possible due to the high sintering temperatures necessary for sufficient mechanical stability of the porous reactor material and that therefore ceramic foams typically have to be coated with the catalyst in a second step. The basic idea of this study is to use flow principles for the placement of catalysts in reactors. A sol-gelation method is applied to directly fabricate a catalytically active porous ceramic from a paste- or gel-like precursor, allowing for the direct precise placement of the catalytic ceramic in a reactor. This promises several advantages compared with the conventional method of coating or impregnating a rigid ceramic foam with a catalytic material in a second step after producing the inert ceramic foam in a first step.

The feasibility of such a sol-gelation foam containing catalytic Rh/ceria/zirconia nanoparticles is tested by its catalytic performance for butane-to-syngas processing. This processing has already been undertaken with the same nanoparticles in the form of packed beds with loose particles[7] and using an improved reactor design.[8] Conventional ceramic foams coated with Rh have already been used for the processing of different hydrocarbons.[9–11] The idea of this study is to use such a small-scale butane-to-syngas processor as part of an entire micro SOFC (Solid Oxide Fuel Cell) system.[12] Butane is a very promising chemical fuel for this purpose due to its high availability and simple storage in liquid phase at low pressure.

Experiments

Preparation of ceramic foam

Nanoparticles made of $Ce_{0.5}Zr_{0.5}O_2$ doped with 2.0 wt % rhodium were prepared in a one-step process by flame spray synthesis as described in previous studies.[7,13–15] To a dry mixture containing 24.1 wt % Rh/ceria/zirconia nanoparticles (average diameter: 10 nm), 72.2 wt % silica sand (Riedel-deHaen, average diameter: 200 μm), 0.9 wt % citric acid salt (triammonium citrate, purum, $\geq$97.0%, Riedel-deHaen) as gelation agent, and 2.8 wt % sodium metasilicate pentahydrate (purum, $\geq$97.0%, Riedel-deHaen) as ceramic binder a similar mass of distilled water was added. The mixture was manually stirred and finally placed in an ultrasonic bath, both steps for about 300 s each. The relatively large silica sand was used as a kind of buffer material to avoid hot spots due to its thermal conductivity, to increase the average pore size, and therefore, to decrease the pressure drop caused by gas flow through the foam-like porous ceramic. The gelation agent causes a gelation or foaming process which leads to a significantly higher porosity at dried state than a comparable packed bed of loose particles, as it is shown below in the results section. The ceramic binder helps all catalytic and SiO_2 particles adhere together and to the reactor wall.

By mixing the solid components with a liquid carrier and by mechanical stirring, a gel- or paste-like, highly viscous suspension could be generated. This paste could be easily applied on a substrate or into a cavity by simply forcing it to flow with a pressurized gas, by coating technologies (e.g., printing techniques), or by any other mechanical or flow application methods. Once the paste was placed on a substrate or in a reactor cavity, the paste was thermally treated. To this end, the paste was heated up to 373 K at a low heating rate of 0.04 K s^{-1} and kept at this temperature for 2 h to evaporate all water inside the gel. The remaining rigid porous ceramic does not need any further thermal or chemical treatment and shows excellent stability avoiding the necessity of sintering at high temperature.

Reactor

This novel method to produce a catalytic porous ceramic was demonstrated in a quartz glass tube (length: 30×10^{-2} m, inner diameter: 2×10^{-3} m, outer diameter: 4×10^{-3} m), where the gel-like foam precursor was pushed to the center of the tube by pressurized air. The tested tubular foam-like reactor (shown in Figure 1) had a reactor volume of 30×10^{-9} m^3 and accordingly a reactor length of 9.6×10^{-3} m. When pushing the wet gel through the tube, no residues of the precursor material remained on the tube wall, as it can be seen in Figure 1.

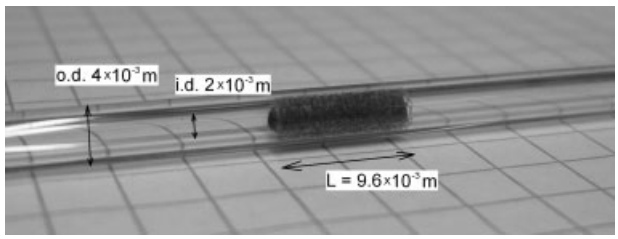

Figure 1. Schematic representation of the foam-like porous ceramic reactor in a quartz glass tube.

Catalyst characterization

The catalytic Rh/ceria/zirconia nanoparticles were characterized in a previous study[7] using the nitrogen adsorption–desorption isotherms, Transmission Electron Microscopy (TEM) and X-ray Diffraction (XRD) techniques. The nitrogen adsorption–desorption isotherms were measured at 77 K with a Tristar (Micromeritics Instruments); the specific surface area of the catalyst was calculated by applying the Brunauer-Emmett-Teller (BET) model on the adsorption isotherm and used to calculate the mean particle diameter.[7] The phase composition and formation of ceria/zirconia mixed oxides was determined by X-ray powder diffraction on a Stowe STADI-P2 (Ge monochromator, Cu $K\alpha_1$, PSD detector).[7] The number of catalytically active Rh surface sites was determined by hydrogen chemisorption using an ASAP 2010 (Micromeritics Instruments). The samples were reduced at 400°C for 90 min using pure hydrogen and cooled down to 40°C under helium atmosphere, as it has been done in a previous study.[8] From the results of hydrogen chemisorption measurements, the metal dispersion was calculated as molecular hydrogen adsorbed dissociatively on Rh metal (H/Rh = 1).[16] Transmission electron micrographs (TEM) of fresh and spent catalyst particles were recorded on a CM30 ST (Philips, 3×10^5 V voltage, point to point resolution 0.19×10^{-9} m) equipped with an energy dispersive X-ray spectrometer (EDX) to analyze the chemical composition of the particles qualitatively. For the TEM and EDX analysis, all samples were dispersed in ethanol, prepared in an ultrasonic bath, and deposited onto a carbon-coated TEM grid.[8] Dried foam reactors were characterized by scanning electron microscopy (SEM).

Test setup

Butane (PanGas, 3.5, 99.95%) was mixed with synthetic air (79% N_2, 21% O_2, PanGas, 5.6, purity of both species: 99.9999%), both at 2.5×10^5 Pa. The flow rates were controlled by Low Delta-P flow meters (Bronckhorst), allowing to operate the reactor slightly above the ambient pressure. The butane/air mixture was fed into the reactor tube placed inside a large tube furnace (MTF 12/38/250, Carbolite). The reactor tube was heated over a length of 30×10^{-2} m,

ensuring practically isothermal conditions inside the reactor placed in the middle of the furnace. The product gas leaving the furnace was maintained at around 388 K to avoid condensation of water. The gas composition was analyzed by a gas chromatograph (6890 GC) coupled with a mass spectrometer (5975 MS, Agilent), using a HP-MOLSIV and a HP-PlotQ column (Agilent), respectively. Helium (PanGas, 5.6, 99.9996%) was added as an internal standard for GC calibration. Under typical run conditions, the molar product gas balances of C, H, and O were closed within 5%.

Catalytic testing procedure

Butane-to-syngas processing was performed in order to test the catalytic behavior of the foam produced by the herein presented sol-gelation method containing catalytic Rh/ceria/zirconia nanoparticles. Using butane and dry air as inlet gas mixture, Partial Oxidation (POX) writes as

$$C_4H_{10} + 2O_2 \rightarrow 5H_2 + 4CO. \quad (1)$$

POX will be the most desirable reaction path for syngas production from hydrocarbons. Another effective reaction for hydrocarbon processing is Steam Reforming (SR), causing butane to react with water:

$$C_4H_{10} + 4H_2O \rightarrow 9H_2 + 4CO. \quad (2)$$

A second water consuming reaction which might take place in a microreactor besides SR is Water Gas Shift (WGS):

$$CO + H_2O \rightarrow H_2 + CO_2. \quad (3)$$

A well-performing butane processor should show high selectivity toward POX products instead of Total Oxidation (TOX) products of butane, which is written as

$$C_4H_{10} + 6.5O_2 \rightarrow 5H_2O + 4CO_2. \quad (4)$$

The reactor was heated from room temperature up to 823 K at a heating rate of 0.21 K s^{-1}. Before the reactor reached the nominal oven temperature of 823 K and the inlet flow of air/butane mixture was started, it was flushed with 3.33×10^{-7} m^3 s^{-1} at STP (standard temperature and pressure) of air for at least 600 s. Each operation point was kept for at least 1200 s before the GC/MS measurement was started to ensure steady state. After the measurements, the tube oven was turned off and the reactor was flushed again with 3.33×10^{-7} m^3 s^{-1} STP of air for about 3600 s while cooling down to 623 K.

The experimental results were analyzed using characteristic values quantifying the catalytic behavior of the catalytic reactor, based on the mole fractions of the outlet gas measured by the GC/MS. The butane conversion η of the microreactor is determined as the molar ratio between converted butane and inlet butane,

$$\eta = \frac{\dot{n}_{C_4H_{10},in} - \dot{n}_{C_4H_{10},out}}{\dot{n}_{C_4H_{10},in}}. \quad (5)$$

The selectivities for hydrogen and carbon monoxide read

$$S_{H_2} = \frac{\dot{n}_{H_2,out}}{\dot{n}_{H_2,out} + \dot{n}_{H_2O,out}} \quad (6)$$

and

$$S_{CO} = \frac{\dot{n}_{CO,out}}{\dot{n}_{CO,out} + \dot{n}_{CO_2,out}}. \quad (7)$$

To quantify the efficiency of the fuel processor, the exergy of inlet and outlet flows were compared, using the definition of molar flow availability $\bar{a}_j$[17]:

$$\bar{a}_j = [(\bar{h}_j(T) - \bar{h}_j(T_0)) - T_0 \times (\bar{s}_j(T) - \bar{s}_j(T_0))] + R \times T_0 \times \ln(X_j) + \bar{a}_j^{chem}, \quad (8)$$

where X_j is the mole fraction of species j. The molar chemical availability $\bar{a}_j^{chem}$ is defined for all necessary species.[18] The absolute molar enthalpies $\bar{h}_j$ and molar entropies $\bar{s}_j$ include the enthalpy and entropy of formation, respectively, and are determined from the so-called JANAF tables.[19] By multiplying the molar flow availabilities with the respective molar flow rates, the hydrogen flow availability $a_{H_2,out}$ the carbon monoxide flow availability $a_{CO,out}$, the total inlet flow availability $a_{tot,in}$, and the total outlet flow availability $a_{tot,out}$ can be calculated, as shown in a previous study.[20] As the herein-presented reactor is considered as a component of an entire micro-SOFC system, hydrogen and carbon monoxide are assumed to be theoretically fully usable by the SOFC and the exergetic efficiency μ_{H_2+CO} only considering H_2 and CO is calculated by

$$\mu_{H_2+CO} = \frac{a_{H_2,out} + a_{CO,out}}{a_{tot,in}}, \quad (9)$$

where the inlet flow availability is practically identical to the chemical exergy of the inlet butane. As an SOFC is able to convert a certain amount of CH_4 and C_4H_{10} in presence of H_2O by internal reforming, the efficiency of the reformer might consider the exergy output of other species than H_2 and CO, which is accounted for by the total exergetic efficiency,

$$\mu_{tot} = \frac{a_{tot,out}}{a_{tot,in}}, \quad (10)$$

where the real exergetic efficiency of the reformer is between μ_{H_2+CO} and μ_{tot}, depending on the performance of the SOFC itself. The C/O ratio or equivalence ratio ϕ based on POX, calculated as

$$\phi = 2 \times \frac{\dot{n}_{C_4H_{10},in}}{\dot{n}_{O_2,in}}, \quad (11)$$

was kept constant at 0.8 for all measurements. It has been proven in previous studies[7,8] that $\phi = 0.8$ is an optimal operating point for butane processing. The total inlet flow rate $\dot{V}_{gas,in}$ was varied during experiments, resulting in a variation of space time τ, defined as the ratio of reactor volume and total volumetric flow rate at the reactor inlet,

$$\tau = \frac{V_{reactor}}{\dot{V}_{gas,in}}. \quad (12)$$

The space time is used as an approximation of the residence time. This approximation implies the assumption of plug flow in the porous reactor, which is reasonable considering that the reactor tube diameter is one order of magnitude larger than the main particle diameter[21] of around 200×10^{-6} m. The Peclet number is defined as

Table 1. Structural and Diffusion Mass Transport Properties of the Foam Reactor

	Total Inlet Flow Rate $\dot{V}_{tot,in}$ [$m^3 s^{-1}$]			
	$\dot{V}_{min} = 3.33 \times 10^{-7}$		$\dot{V}_{max} = 6.67 \times 10^{-7}$	
C_4H_{10} reaction rate $r_{C_4H_{10}}$ [mol kg^{-1} s^{-1}]	2.54×10^{-2}		4.94×10^{-2}	
	Outlet	Inlet	Outlet	Inlet
C_4H_{10} concentration $C_{C_4H_{10}}$[mol m^{-3}]	9.22×10^{-2}	1.189	9.24×10^{-2}	1.189

	SiO_2 Particles		Rh/ceria/zirconia Particles	
	Min	Max	Min	Max
Pore diameter d_{pore} [m]	10×10^{-6}	50×10^{-6}	1×10^{-9}	5×10^{-9}
Knudsen number [–]	2.22×10^{-3}	1.11×10^{-3}	22.2	110.8
Molecular diffusivity D_m [m^2 s^{-1}]	6.19×10^{-5}			
Knudsen diffusivity D_{Kn} [m^2 s^{-1}]	1.83×10^{-3}	9.13×10^{-3}	1.83×10^{-7}	9.13×10^{-7}
Combined diffusivity D_{comb} [m^2 s^{-1}]	5.99×10^{-5}	6.15×10^{-5}	3.21×10^{-8}	1.59×10^{-7}
Porosity ε [–]	0.60		0.42	
Effective diffusivity D_{eff} [m^2 s^{-1}]	2.16×10^{-5}	2.21×10^{-5}	3.21×10^{-8}	1.59×10^{-7}
Bulk density ρ_{bulk} [kg m^{-3}]	1250		2690	
Characteristic length L_{char} [m]	3.33×10^{-5}		1.67×10^{-9}	

	SiO_2 Particles		Rh/ceria/zirconia Particles	
	Min*	Max*	Min*	Max*
Weisz modulus Φ [–] $\dot{V}_{min} = 3.33 \times 10^{-7}$ m^3 s^{-1}	1.34×10^{-3}	1.78×10^{-2}	1.00×10^{-9}	6.42×10^{-8}
Weisz modulus Φ [–] $\dot{V}_{max} = 6.67 \times 10^{-7}$ m^3 s^{-1}	2.60×10^{-3}	3.45×10^{-2}	1.95×10^{-9}	1.25×10^{-7}

*For the minimal Weisz modulus, the maximal effective diffusivity of the specific level and the C_4H_{10} concentration at the inlet for the specific flow rate have to be taken into account. For the maximum Weisz modulus, the minimal effective diffusivity of the specific level and the C_4H_{10} concentration at the outlet for the specific flow rate have to be taken into account. Calculation example:

$$\Phi_{min}(\text{Rh/ceria/zirconia particles}, \dot{V}_{min}) = \frac{r_{C_4H_{10}}(\dot{V}_{min}) \times \rho_{bulk,\,Rh/ceria/zirconia} \times (L_{char,\,Rh/ceria/zirconia})^2}{C_{C_4H_{10},inlet}(\dot{V}_{min}) \times D_{eff,max,Rh/ceria/zirconia}} =$$

$$= \frac{2.54 \times 10^{-2} \times 2690 \times (1.67 \times 10^{-9})^2}{1.189 \times 1.59 \times 10^{-7}} = 1.00 \times 10^{-9}$$

$$Pe = \frac{u \times d_{tube}}{D_{eff}}, \tag{13}$$

where u is the Darcy velocity and D_{eff} the effective diffusivity of butane in the porous medium. With D_{eff} from Table 1, the Peclet number is 40.2. This indicates that mass transport in the porous medium is dominated by the axial convection instead of radial dispersion.[21] Thus, the assumption of plug flow is valid. Furthermore, the effect of the shear force by the reactor wall on the radial velocity profile can be evaluated using the shear boundary thickness δ, depending on the gas permeability κ of the porous medium[22]:

$$\delta \sim \sqrt{\kappa}. \tag{14}$$

Results

Structural analysis of porous ceramic

The bulk density of the catalytic bed (including all pores) was determined as 1250 kg m^{-3} by measuring the volume and the mass of the reactor. The skeletal density (excluding all pores) of the solid material including silica sand and catalytic nanoparticles was calculated to be 3130 kg m^{-3}, leading to a volumetric porosity of 60.0%. Accordingly, the tested reactor of 30×10^{-9} m^3 contained 9.0×10^{-3} g of catalytic Rh/ceria/zirconia nanoparticles.

The pressure drop during the operation of the foam-like reactor was measured continuously and the average pressure drop for each flow rate is shown for the tested reactor in Figure 2. The flow rate $\dot{V}$ is averaged between the inlet and outlet conditions. Because of the low velocities in the

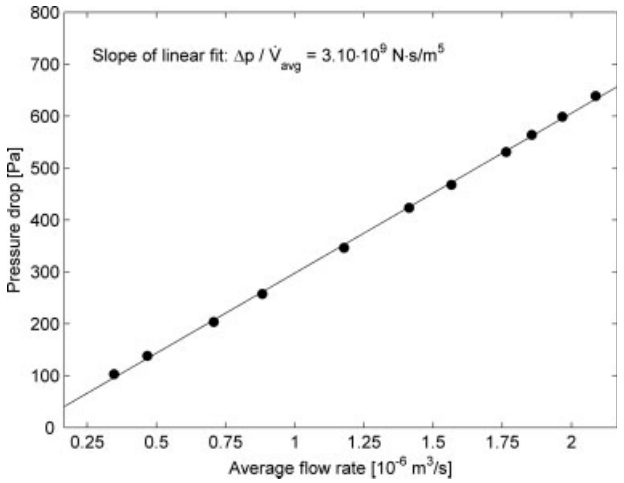

Figure 2. Pressure drop through the reactor of 30×10^{-9} m^3 during butane-to-syngas processing as a function of the averaged gas flow rate.

Figure 3. SEM image of the porous ceramic showing silica sand particles in the order 200 × 10^{-6} m and larger pores between them.

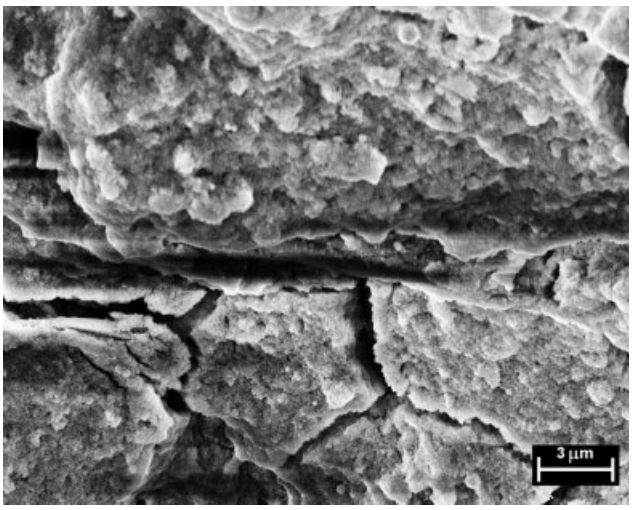

Figure 4. SEM image showing cracks and pores in the catalytic layer covering the larger silica particles.

reactor, the pressure drop Δp shows good agreement to the linearity proposed by Darcy's Law,

$$\Delta p = \frac{v \times \rho}{\kappa} \times \frac{L}{A} \times \dot{V}. \tag{15}$$

The gas permeability κ is calculated to 3.42 × 10^{-11} m^2. The pressure drop Δp and the flow rates at inlet and outlet were measured, and the values of kinematic viscosities v and densities ρ are calculated from the measured gas composition, averaged between inlet and outlet of the reactor. A is the known cross-sectional area and L the known length of the reactor. Using the calculated gas permeability, the thickness of the shear boundary layer can be estimated to be 5.8 × 10^{-6} m. This is around 170 times lower than the tube radius and shows again that the effect of the wall shear can be neglected and the assumption of a uniform radial velocity profile is well feasible.[22]

In SEM images, the structure of the silica particles of 200 × 10^{-6} m average diameter can be distinguished very well with pores of some tens of microns between them (Figure 3). On the surface of these large silica particles, cracks and pores of the order of 1 × 10^{-6} m can be detected (Figure 4). The relatively large SiO_2 particles are homogeneously covered with a thin layer of Rh/ceria/zirconia nanoparticles (Figure 5a). For better comparison, a mechanically and intentionally destroyed part of the foam is shown in Figure 5b. On the right, a SiO_2 particle is partly covered with a nanoparticle layer and on the left, the smooth surface of the blank and uncoated SiO_2 particle is visible.

For its use as a catalyst material for any chemical reaction process, e.g., for butane-to-syngas processing, it is essential to know if the reactor operates in a reaction-limited or diffusion-limited regime. To better investigate the mass transport limitation of the presented foam-like reactor, the Weisz modulus for multi-scale systems (Table 1) is evaluated similarly to earlier studies.[23] From SEM images (Figures 3–5), two critical levels can be estimated: On the one hand, the coarse structure of the foam reactor is determined by SiO_2 sand particles of 200 × 10^{-6} m average diameter with pores in the order of 10–50 × 10^{-6} m between them. On the other hand, these large particles are covered with a thin layer of catalytic nanoparticles of 10 × 10^{-9} m average diameter. This catalytic layer has been assumed to be a close packed bed of

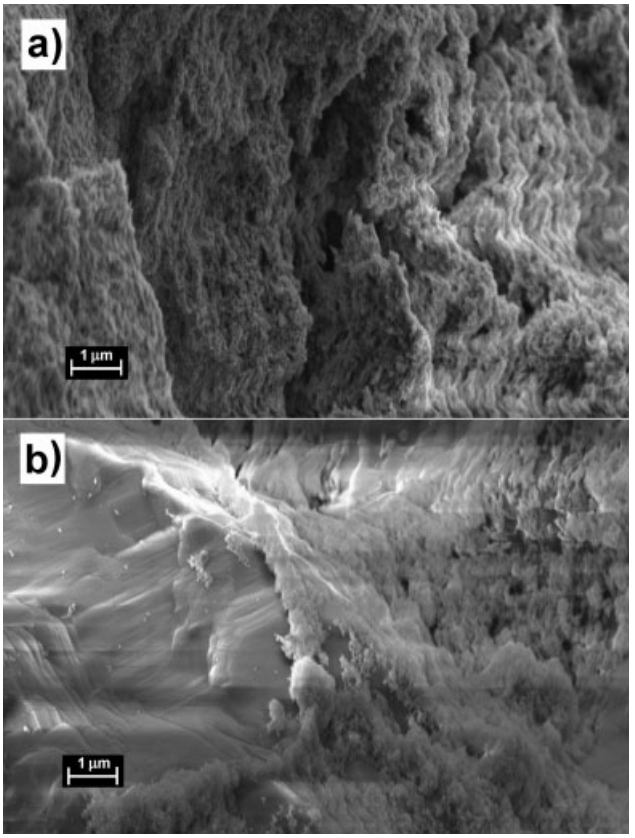

Figure 5. SEM image showing (a) the catalytic layer consisting of nanoparticles with a porous surface and (b) a partly covered SiO_2 particle for comparison.

Table 2. Average ($\bar{j}$), Standard Deviation (σ_j), and Relative Fluctuation (rel. fluct. $= \sigma_j/\bar{j}$) of Butane Conversion, Hydrogen Selectivity, and Carbon Monoxide Selectivity for Inlet Flow Rates of 3.33, 5.00, and 6.67 $\times$ 10^{-7} m^3 s^{-1} at Standard State

Total Inlet Flow Rate	Butane Conversion			Hydrogen Selectivity			Carbon Monoxide Selectivity		
$\dot{V}_{tot,in}$[m^3 s^{-1}]	$\bar{\eta}$	σ_η	rel. fluct.	$\overline{S_{H2}}$	$\sigma_{S_{H2}}$	rel. fluct.	$\overline{S_{CO}}$	$\sigma_{S_{CO}}$	rel. fluct.
3.33 $\times$ 10^{-7}	86.5%	0.45%	0.52%	88.1%	0.27%	0.30%	67.2%	0.29%	0.43%
5.00 $\times$ 10^{-7}	84.2%	0.20%	0.24%	88.5%	0.11%	0.13%	69.6%	0.26%	0.37%
6.67 $\times$ 10^{-7}	84.0%	0.34%	0.40%	89.3%	0.13%	0.15%	72.7%	0.16%	0.22%

spherical particles with a pore diameter of 1–5 $\times$ 10^{-9} m. In Table 1, the Weisz modulus Φ, which is defined as

$$\Phi = \frac{r_{C_4H_{10}} \times \rho_{bulk} \times L_{char}^2}{C_{C_4H_{10}} \times D_{eff}}, \tag{16}$$

is evaluated for these two levels and for two different total inlet flow rates (3.33 and 6.67 $\times$ 10^{-7} m^3 s^{-1}). The butane reaction rate $r_{C_4H_{10}}$ was calculated for both flow rates and the butane concentration $C_{C_4H_{10}}$ measured at the inlet and the outlet. The combined diffusivity D_{comb} is calculated for the minimal and maximal pore diameter estimated before, taking molecular and Knudsen diffusion into account:

$$D_{comb} = \left(\frac{1}{D_m} + \frac{1}{D_{Kn}}\right)^{-1}. \tag{17}$$

The molecular diffusion D_m of butane in air is estimated by the Chapman-Enskog equation,[24]

$$D_m = 5.96 \times 10^{-24} \times T^{3/2} \times \frac{\sqrt{\frac{1}{M_{C_4H_{10}}} + \frac{1}{M_{air}}}}{p \times \sigma_{12}^2 \times \Omega}, \tag{18}$$

where the values for σ_{12} (= 4.199 $\times$ 10^{-10} m) and Ω (= 0.8823) are taken from literature.[24] For the temperature T, the nominal reactor temperature of 823 K is used. All parameters in Eq. 18 are used in SI units. The Knudsen diffusivity D_{Kn} reads[24]:

$$D_{Kn} = 48.5 \times d_{pore} \times \sqrt{\frac{T}{M_{C_4H_{10}}}}, \tag{19}$$

Considering the porosity of both levels, the effective diffusivity D_{eff} can be calculated[23]:

$$D_{eff} = \varepsilon^2 \times D_{comb}. \tag{20}$$

The porosity and the bulk density of the overall regime were measured and already shown before. For the layer of nanoparticles, a close package is assumed, leading to a porosity of 0.42 and a bulk density of the nanoparticles ρ_{bulk} of 2690 kg m^{-3}. Finally, the characteristic length L_{char} is estimated for spherical particles[23]:

$$L_{char} = d_{particle}/6. \tag{21}$$

As the resulting values show for both flow rates and both levels, the Weisz modulus is significantly lower than unity ($\Phi \ll 1$). Therefore, the reactor is operated in a reaction-limited regime. The diffusion limitation is negligible compared with the reaction rate of butane conversion. For the first level of the larger silica particles, the Weisz modulus is between 1.34 $\times$ 10^{-3} and 1.78 $\times$ 10^{-2} for the lower tested flow rate (Table 1). By increasing the flow rate to the highest flow rate tested, the Weisz modulus almost doubles. Nevertheless, even for the most conservative estimation and the highest flow rate, the Weisz modulus is below 3.5 $\times$ 10^{-2}. For the second level, considering the gas diffusion in the layer of nanoparticles, the reaction rate is 7–9 orders of magnitude faster than the diffusive mass transport.

Catalytic stability test

Before investigating the effect of operational parameters on the catalytic performance of the foam-like reactors, the catalytic stability of a reactor was tested. Within the first hour of operation, the catalytic behavior was slightly unstable. After 1 hour however, the catalytic performance was very stable for several days of measurement. In Table 2, the resulting butane conversion, hydrogen selectivity, and carbon monoxide selectivity are evaluated for three different inlet flow rates. The average ($\bar{j}$) and the standard deviation (σ_j) of these three characteristic results are calculated over the tested period of 5 h each and the fluctuation of the catalytic performance is indicated by a relative fluctuation (rel.fluct.), which is the standard deviation divided by the mean value of the different results. Table 2 shows excellent stability during these measurements with a maximum relative fluctuation of 0.52%. Porous ceramic reactors have been tested for up to 40 h of operation without showing any deactivation of the catalyst. The structure and the surface of the nanoparticles after 40 h of operation are analyzed by taking TEM images clearly showing no change of the structure of the nanoparticles compared with TEM images of the fresh catalyst (Figure 6). EDX measurements showed no change of the chemical composition of the nanoparticles before and after usage as catalyst for 40 h, especially indicating that no carbon deposition on the nanoparticles took place during the hydrocarbon reforming, as it has been shown in earlier studies.[7,8]

Effect of inlet flow rate and space time

In Figure 7, the measured catalytic performance as a function of the inlet flow rate of butane/air mixture is shown for a foam reactor made by the herein presented in-situ sol-gelation method. The butane conversion decreases with increasing flow rate (Figure 7a). The butane conversion stays between 83% and 84% even for the highest flow rates. The selectivities toward hydrogen and carbon monoxide show similarly: No maximum is reached for the 30 $\times$ 10^{-9} m^3 reactor within the tested range from 3.33 to 6.67 $\times$ 10^{-7} m^3 s^{-1}. The hydrogen selectivity increases almost linearly from 85% to 89% for the tested flow rates (Figure 7a), which is

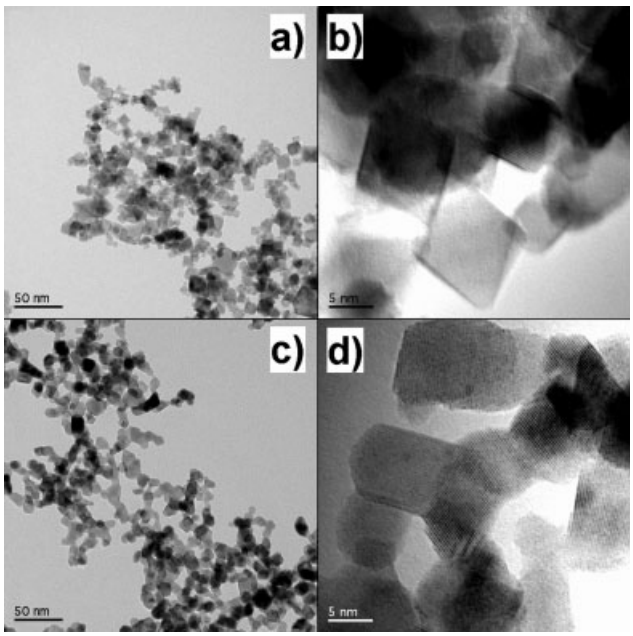

Figure 6. TEM images showing the catalyst (a) and (b) before usage and (c) and (d) after 40 h of operation.

an excellent result considering the low operating temperature of 823 K. For the investigated reactor, almost 73% carbon monoxide selectivity can be achieved (Figure 7a).

For the reactor of 30×10^{-9} m^3, the exergetic efficiency μ_{H_2+CO} increases from 48% to 59% for the highest flow rates, as it can be seen in Figure 7b, if only hydrogen and carbon monoxide are accounted for. The total exergetic efficiency μ_{tot} is significantly higher than μ_{H_2+CO} mainly due to unconverted butane.

Next, the same results are plotted as function of space time to better account for the effect of this characteristic parameter (Figure 8). The butane conversion decreases with decreasing space time (Figure 8a). Both selectivities increase monotonically for shorter space times without reaching an optimum within the investigated range of flow rates and space times (Figure 8a).

As the inlet gas flow of butane as fuel increases for shorter space times, the absolute exergy of the product gas usable for the SOFC in form of hydrogen and carbon monoxide grows with decreasing space time and increasing reactor volume, as it can be seen in Figure 8b. Hydrogen and carbon monoxide with an exergy or flow availability of 3.58 W can be produced at a space time of 17×10^{-3} s,

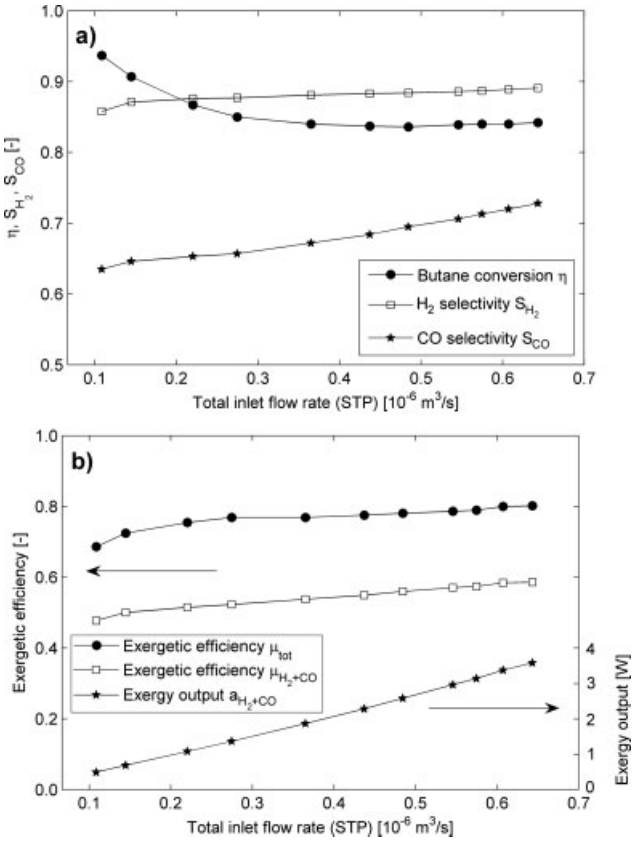

Figure 7. (a) Butane conversion, hydrogen selectivity, and carbon monoxide selectivity, and (b) exergetic efficiency of a foam reactor with 30 $\times$ 10^{-9} m^3 reactor volume for different flow rates.

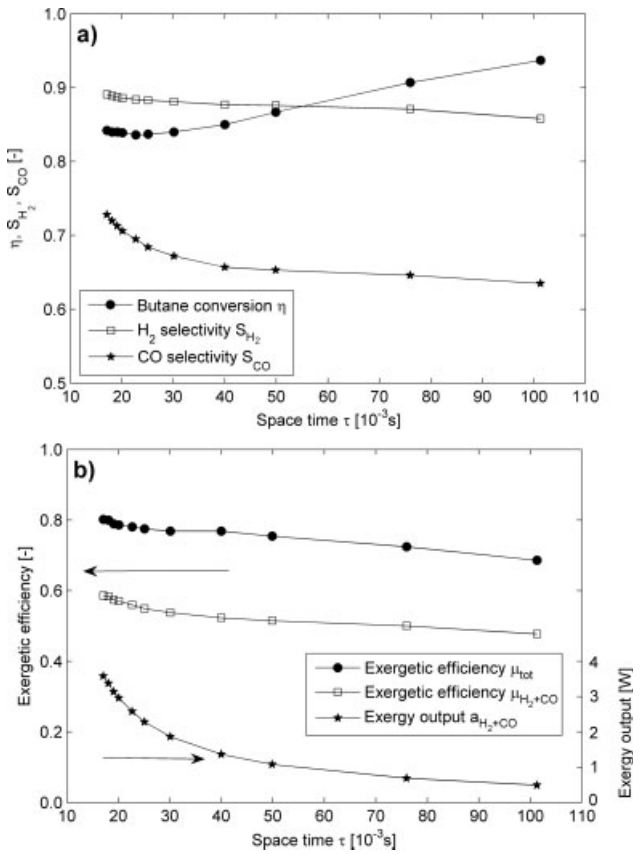

Figure 8. (a) Butane conversion, hydrogen selectivity, and carbon monoxide selectivity, and (b) exergy of the product gas in form of hydrogen and carbon monoxide for a reactor with 30 $\times$ 10^{-9} m^3 reactor volume for different space times.

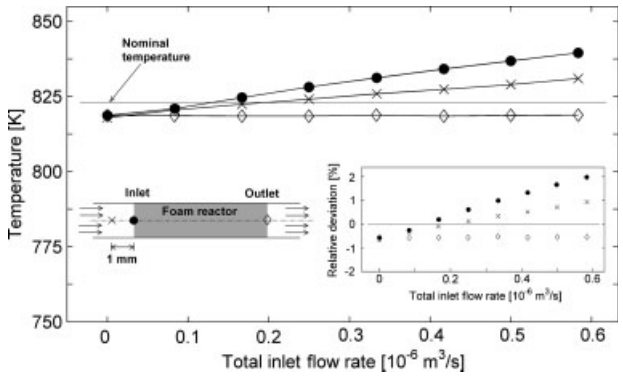

Figure 9. Temperatures at three different positions (inlet, outlet, and 1 mm before the inlet) of the reactor of 30×10^{-9} m^3 and the resulting deviation relative to the nominal reactor temperature as functions of the inlet gas flow rate.

indicating a power density of 120 MW m^{-3}. The exergy output increases dramatically for space times below 40×10^{-3} s.

Reactor temperature

To achieve isothermality, the reactor tube is placed in a large tube furnace operating at a nominal temperature of 823 K. The outer surface area of the reactor tube is relatively large compared with the small foam reactor (see Figure 1) and the low gas flow rates, allowing for considerable heat transfer from the tube to the ambient, and quartz has a fairly high thermal conductivity. The silica sand inside the foam helps to avoid local hot spots inside the reactor and enhances thermal dissipation.

To prove the assumption of a practically isothermal reactor, the temperature is measured by three thermocouples. The first one is positioned 1×10^{-3} m upstream in front of the porous ceramic reactor material, the two other thermocouples are placed right at the surface of the ceramic at the inlet and the outlet. The temperatures are shown for different inlet flow rates of butane/air mixture up to 5.85×10^{-7} m^3 s^{-1} and a reactor volume of 30×10^{-9} m^3 (Figure 9). Without any gas flow or with only air flowing through the reactor, the temperatures amount everywhere to 818.7 K, slightly below the nominal temperature of 823 K. The temperature at the end of the reactor stays constant at around 818.7 K for all flow rates, whereas the temperatures at the beginning and 1×10^{-3} m upstream in front of the reactor increase with higher flow rates. However, even for the highest flow rate tested in this study, the temperature at the entrance of the reactor is only increased by about 16 K. As the most exothermic reactions consume oxygen, the hottest region of the reactor can be supposed to be close to the entrance, exactly where we measure the temperature.

To obtain a better impression of the effect of the low temperature variation within the reactor on the catalytic performance, the influence on butane conversion is analyzed analytically. From experimental data on the temperature dependence of the butane conversion on the present Rh/ceria/zirconia nanoparticles and under the same operating conditions, as shown in an earlier study,[7] the relative change in butane conversion rate constant $k(T_2)/k(T_1)$ can be calculated as 1.2055 for the temperature range between $T_1 = 798$ K and $T_2 = 873$ K. Using an Arrhenius-type equation, the butane conversion rate constant reads:

$$k(T) \sim \exp\left(-\frac{E_a}{R \times T}\right). \tag{22}$$

This leads to an apparent activation energy E_a of around 14.44 kJ mol^{-1} for the consumption of butane.

Considering the nominal temperature of 823 K, the absolute temperature deviation of 16 K results in a low relative deviation of 2%. When the calculated apparent activation energy for butane conversion is used for the measured temperature variation of 16 K, the butane conversion rate k experiences a relative variation or deviation of 4.2%. Therefore, the assumption of practically isothermal conditions is clearly acceptable, as the temperature distribution and the resulting butane conversion vary less than 2% and 4.2%, respectively, in the worst case scenarios.

Discussion

In addition to the reduction in process complexity, the herein proposed method offers advantages over the conventional two-step method of coating or impregnating a rigid ceramic foam with a liquid catalyst precursor.

First, in contrast to the impregnation of a rigid ceramic foam, the catalyst can be easily added to a liquid carrier and dispersed homogeneously by mixing and stirring. Second, this method avoids the existence of loose or dry particles during the production of the porous ceramic as well as during its catalytic operation after drying. The usage of loose particles is delicate or even impossible for clean room production techniques and might cause severe health risks. The method presented herein eliminates the problem of polluting the ambient by nanoparticles during production and operation. The dried porous ceramic coheres very well together and does not require any kind of filters or ceramic fiber plugs to fix its position. The catalytic nanoparticles cannot erode from the reactor, which is a crucial problem in packed bed reactors consisting of loose particles. The dry and rigid foam-like ceramic adheres well to the substrate or reactor wall without any gap or void space in between. This avoids bypassing of gas around the catalytic material.

Finally, the foam-like ceramic can be transported using flow principles, as described earlier, in the form of a paste-like precursor to its desired position on a substrate or in a reactor. Especially when dealing with a reactor of varying cross section in small-scale applications (typically a smaller cross section at the inlet and the outlet of the reactor), this is a crucial advantage of the foam-like ceramic. These small-scale reactors are typically made of micromachined wafers that have to be bonded together. After the wafers are bonded together it is impossible to introduce a rigid foam into such a reactor through the smaller inlet or outlet. Introducing the foam before the bonding procedure is often difficult or impossible because the rigid foam and loose nanoparticles are often incompatible with clean room conditions required for the bonding.

Structural analysis of porous ceramic

The analysis of the ceramic reactor proves that the herein presented foam-like ceramic has very appropriate properties for a catalytic reactor material: an intermediate porosity of 60%, an excellent thermal and chemical stability up to 1123 K, and a homogenous distribution of catalytic active material. The porosity is a crucial parameter for an efficient reactor: on the one hand, low porosity and therefore small pore sizes increase the pressure drop of a gas flow through the reactor; on the other hand, the void volume has to be limited to provide a large catalytically active surface area. This requirement is fulfilled by the foam-like ceramic due to its multi-scale pores: larger pores of several tens of microns (Figure 3) and smaller of the order of 1×10^{-6} m (Figures 4 and 5a) allow for a high convective mass transport at a reasonably low pressure drop, whereas the nanoporous and completely covering layer of catalytic nanoparticles leads to a large surface-to-volume ratio and a low diffusive mass transport resistance. The performance of the reactor is clearly reaction-limited and the diffusion limitation is low or even negligible, as evaluated by using an analysis of the Weisz modulus (Table 1) for the larger pores between the silica sand particles and for the layer of catalytic nanoparticles covering the silica.

Considering the very simple and fast manufacturing procedure, the presented method of producing a catalytic porous ceramic by a direct sol-gelation method in-situ in the final reactor geometry instead of a conventional impregnation of a ceramic supporting foam with a catalyst precursor shows all characteristics necessary for a catalytic reactor material.

Catalytic stability test

An essential requirement of a catalytic reactor for significant measurements as well as for potential usage in an industrial application is the catalytic stability. All reactors of this study are investigated for at least 40 h of operation without any sign of catalyst deactivation or erosion (Figure 6 and Table 2). Similar to earlier results of the same catalytic nanoparticles,[7,8] the catalyst does not require any pretreatment to reduce the nanoparticles by contact with an H_2-rich gas flow, as usually done for such catalysts.[25–28] One advantage of the herein-used catalytic nanoparticles is that no such pretreatment is necessary, because the catalytic activity of the Rh/ceria/zirconia is strong enough from the beginning to convert butane to hydrogen and carbon monoxide. After about 1 h of fluctuating catalytic performance, all reactors show very stable operation.

The catalytic stability is a sign that carbon deposition on the catalyst is not a significant problem for the used catalyst for partial oxidation of butane, as it has already been suggested in a previous study.[8] This finding is strongly confirmed by the results of EDX measurements proving that not significant carbon deposition takes place. The carbon mass balance for each GC/MS measurement does not show any soot formation in the reactors either.

Effect of inlet flow rate and space time

The results of the catalytic activity show that the structural and chemical properties of the foam-like ceramic supporting the catalytic nanoparticles do not reduce or interfere with its catalytic performance. The catalytic activity of the porous ceramic reactors is as excellent as for packed bed reactors containing the same catalyst as loose particles.[7,8] Maximal selectivities toward hydrogen of 89% and carbon monoxide of 74%, respectively, at a simultaneous butane conversion of 84% for the highest inlet flow rate of 6.67×10^{-7} m^3 s^{-1} (Figure 7a), referring to a short contact or space time of 17×10^{-3} s (Figure 8a), prove excellent catalytic activity and the ability to efficiently process butane. The production of hydrogen and carbon monoxide within a microreactor with a calculated exergy density of 120 MW m^{-3} is a remarkable result, considering the low reaction temperature of 823 K. This result is very close to the overall catalytic performance measured for the same catalytic nanoparticles used in a conventional packed bed of loose particles[8]: For a total inlet flow rate of 5.00×10^{-7} m^3 s^{-1} and a slightly higher catalyst loading (10×10^{-3} g instead of 9×10^{-3} g in the present study), butane conversion of 90%, hydrogen selectivity of 81%, and carbon monoxide selectivity of 66% were measured. The slightly lower butane conversion and higher selectivities for the present study can be explained by the higher inlet flow rate due to the resulting lower space time, as it has been shown before.[8] This catalytic performance is excellent compared with other catalysts considering the low operating temperature, as it has been discussed in detail.[7,8]

From the results shown here, it can be expected that the selectivities toward hydrogen and carbon monoxide reach maxima for a 30×10^{-9} m^3 reactor at flow rates significantly above 6.67×10^{-7} m^3 s^{-1} inlet flow rate (Figure 7a), which is beyond the range tested for this study. These results confirm the earlier conclusion from the calculated Weisz modulus that the reactor is not operated in a mass transfer limited regime, but rather in a reaction-limited regime.

Reactor temperature

An essential objective of this study is to investigate the processing of butane at a relatively low temperature of 823 K without large temperature gradients in the reactor. This is important for an appropriate analysis of the catalytic behavior of the foam-like ceramic and especially critical for a potential application in small electronic devices. The results clearly show that the reactors can be operated at practically isothermal conditions with maximal temperature differences of 16 K, indicating a small relative error of about 2% when compared with the nominal operating temperature of 823 K (Figure 9). The deviation in catalytic performance, which is strongly temperature dependent, is insignificant: The maximum deviation of the butane conversion rate compared with its value at the nominal temperature is only 4.2% and the assumption of a practically isothermal reactor is feasible. This is due to the reactor design allowing for sufficient heat transfer between the reactor and the ambient via thermal conduction through the reactor tubes in axial and radial direction. Although most studies on hydrocarbon processing focus on well insulated or practically adiabatic reactors in which necessarily large temperature gradients occur within the reactor and in the gas flow itself,[29–31] the configuration chosen for this work reflects the necessity of small

temperature differences in practical applications to reduce thermal stress and thermomechanical failure.

Conclusion

In this study, a novel method is introduced to fabricate a porous foam-like ceramic containing catalytic nanoparticles by a direct and one-step sol-gelation procedure. With this simple and fast method, a liquid precursor already containing the catalyst can be introduced by flow techniques into the final reactor geometry, avoiding the common procedure of impregnating or coating a substrate with the catalytic material. The porous ceramic made by sol-gelation demonstrates excellent properties for a catalytic reactor material, e.g., a low pressure drop due to its porosity of approximately 60% and good thermal and chemical stability.

To prove the high catalytic activity and stability of the foam-like reactor, the reaction of butane to syngas is investigated on Rh/ceria/zirconia nanoparticles in porous ceramic reactors. The maximal hydrogen selectivity amounts to 89% and the carbon monoxide selectivity to 74% at a butane conversion of 84% for the tested reactor of 30×10^{-9} m^3 reactor volume and the highest inlet flow rate of 6.67×10^{-7} m^3 s^{-1}. This corresponds to a flow availability in form of hydrogen and carbon monoxide of 3.58 W at an exergetic efficiency μ_{H_2+CO} of 59%, which is an excellent result for the low operating temperature of 823 K.

The effect of operating parameters such as the inlet flow rate on the hydrocarbon processing is analyzed and it is shown that the reactor is operated in the fully reaction-limited regime for the tested conditions. Diffusion mass transport limitations are negligible for the investigated cases.

Acknowledgements

This work was financially supported by the following Swiss institutions: Commission for Technology and Innovation (CTI), Center of Competence Energy and Mobility (CCEM), Swiss Federal Office of Energy (SFOE), and Swiss Electric Research. The technical support from the LTNT team (Jovo Vidic) is gratefully acknowledged.

Notation

A = cross-sectional area (m^2)
a = flow availability or exergy (W)
$\bar{a}$ = molar flow availability or exergy (J mol^{-1})
C = molar concentration (mol m^{-3})
d = diameter (m)
D = diffusivity (m^2 s^{-1})
E_a = apparent activation energy (J mol^{-1})
$\bar{h}$ = absolute flow enthalpy (J mol^{-1})
k = reaction rate constant (s^{-1})
L = length (m)
M = molecular weight (kg mol^{-1})
$\dot{n}$ = molar flow rate (mol s^{-1})
n_{cat} = number of catalytically active surface sites (mol)
p = absolute pressure (Pa)
Δp = pressure drop (Pa)
Pe = Peclet number
r = reaction rate (mol kg^{-1} s^{-1})
R = universal gas constant (8.3145 J mol^{-1} K^{-1})
$\bar{s}$ = absolute molar entropy (J mol^{-1})
$S_{H_2/CO}$ = hydrogen/carbon monoxide selectivity
T = absolute temperature (K)
u = Darcy velocity (m s^{-1})
V = volume (m^3)
$\dot{V}$ = volumetric flow rate (m^3 s^{-1})
X = mole fraction

Greek letters

ε = porosity
δ = shear boundary layer thickness (m)
η = butane conversion
ϕ = equivalence or C/O ratio
κ = permeability (m^2)
μ = exergetic efficiency
ρ = density (kg m^{-3})
σ = standard deviation
σ_{12} = collision diameter (m)
τ = space time (s)
ν = kinematic viscosity (m^2 s^{-1})
Φ = Weisz modulus
Ω = collision integral

Literature Cited

1. Schimmoeller B, Schulz H, Pratsinis SE, Bareiss A, Reitzmann A, Kraushaar-Czarnetzki B. Ceramic foams directly-coated with flame-made V_2O_5/TiO_2 for synthesis of phthalic anhydride. *J Catal*. 2006;243:82–92.
2. Reitzmann A, Patcas FC, Kraushaar-Czarnetzki B. Ceramic sponges—application potential of monolithic network structures as catalytic packages. *Chem Ing Tech*. 2006;78:885–898.
3. Snijkers F, Mullens S, Buekenhoudt A, Vandermeulen W, Luyten J. Ceramic foams coated with zeolite crystals. *Funct Graded Mater VIII*. 2005;492–493:299–303.
4. Twigg MV, Richardson JT. Fundamentals and applications of structured ceramic foam catalysts. *Ind Eng Chem Res*. 2007;46:4166–4177.
5. Liguras DK, Goundani K, Verykios XE. Production of hydrogen for fuel cells by catalytic partial oxidation of ethanol over structured Ni catalysts. *J Power Sources*. 2004;130(1–2):30–37.
6. Hotz N, Poulikakos D, Studart A, Bieberle-Hütter A, Gauckler LJ. Porous ceramic catalysts and methods for their production and use. Patent EP 08 012273.2, 2008.
7. Hotz N, Stutz MJ, Loher S, Stark WJ, Poulikakos D. Syngas production from butane using a flame-made $Rh/Ce_{0.5}Zr_{0.5}O_2$ catalyst. *Appl Catal B: Environ*. 2007;73(3–4):336–344.
8. Hotz N, Osterwalder N, Stark WJ, Bieri NR, Poulikakos D. Disk-shaped packed bed micro-reactor for butane-to-syngas processing. *Chem Eng Sci*. 2008;63:5193–5201.
9. Panuccio GJ, Williams KA, Schmidt LD. Contributions of heterogeneous and homogeneous chemistry in the catalytic partial oxidation of octane isomers and mixtures on rhodium coated foams. *Chem Eng Sci*. 2006;61:4207–4219.
10. Panuccio GJ, Dreyer BJ, Schmidt LD. A comparison of the catalytic partial oxidation of C-1 to C-16 normal paraffins. *AIChE J*. 2007;53:187–195.
11. Williams KA, Horn R, Schmidt LD. Performance of mechanisms and reactor models for methane oxidation on Rh. *AIChE J*. 2007;53:2097–2113.
12. Bieberle-Hütter A, Beckel D, Infortuna A, Muecke UP, Rupp JLM, Gauckler LJ, Rey-Mermet S, Muralt P, Bieri NR, Hotz N, Stutz MJ, Poulikakos D, Heeb P, Mueller P, Bernard A, Gmuer R, Hocker T. A micro-solid oxide fuel cell system as battery replacement. *J Power Sources*. 2008;177:123–130.
13. Stark WJ, Madler L, Maciejewski M, Pratsinis SE, Baiker A. Flame synthesis of nanocrystalline ceria-zirconia: effect of carrier liquid. *Chem Commun*. 2003;5:588–589.
14. Stark WJ, Maciejewski M, Madler L, Pratsinis SE, Baiker A. Flame-made nanocrystalline ceria/zirconia: structural properties and dynamic oxygen exchange capacity. *J Catal*. 2003;220:35–43.
15. Stark WJ, Grunwaldt JD, Maciejewski M, Pratsinis SE, Baiker A. Flame-made Pt/ceria/zirconia for low-temperature oxygen exchange. *Chem Mater*. 2005;17:3352–3358.
16. Montini T, Condo AM, Hickey N, Lovey FC, De Rogatis L, Fornasiero P, Graziani M. Embedded Rh(1 wt.%)@Al_2O_3: effects of high temperature and prolonged aging under methane partial oxidation conditions. *Appl Catal B: Environ*. 2007;73:84–97.

17. Moran MJ, Shapiro HN. *Fundamentals of Engineering Thermodynamics* (4th edition). New York: Wiley, 1999.
18. Morris DR, Szargut J. Standard chemical exergy of some elements and compounds on the planet earth. *Energy*. 1986;11:733–755.
19. Chase MW. NIST-JANAF thermochemical tables (4th edition). *J Phys Chem Ref Data*. 1998;Monograph 9:1–1951.
20. Hotz N, Senn SM, Poulikakos D. Exergy analysis of a solid oxide fuel cell micropowerplant. *J Power Sources*. 2006;158:333–347.
21. Crawshaw JP, Paterson WR, Scott DM. Gas residence time distribution studies of fixed, moving and frozen beds of spheres. *Chem Eng Res Des*. 1993;71(A6):643–648.
22. Webb SW. Gas transport mechanisms. In: Ho CK, Webb SW, editors. *Gas Transport in Porous Media*. Dordrecht: Springer, 2006:5–26.
23. Heinrichs B, Pirard JP, Schoebrechts JP. Mass transfer in low-density xerogel catalysts. *AIChE J*. 2001;47:1866–1873.
24. Cussler EL. *Diffusion, Mass Transfer in Fluid Systems* (2nd edition). Cambridge: Cambridge University Press, 1997.
25. Huff M, Schmidt LD. Production of olefins by oxidative dehydrogenation of propane and butane over monoliths at short-contact times. *J Catal*. 1994;149:127–141.
26. Laosiripojana N, Assabumrungrat S. Hydrogen production from steam and autothermal reforming of LPG over high surface area ceria. *J Power Sources*. 2006;158:1348–1357.
27. Schneider A, Mantzaras J, Jansohn P. Experimental and numerical investigation of the catalytic partial oxidation of CH_4/O_2 mixtures diluted with H_2O and CO_2 in a short contact time reactor. *Chem Eng Sci*. 2006;61:4634–4649.
28. Silberova B, Venvik HJ, Holmen A. Production of hydrogen by short contact time partial oxidation and oxidative steam reforming of propane. *Catal Today*. 2005;99(1–2):69–76.
29. Hickman DA, Schmidt LD. Production of syngas by direct catalytic-oxidation of methane. *Science*. 1993;259:343–346.
30. Horn R, Williams KA, Degenstein NJ, Bitsch-Larsen A, Nogare DD, Tupy SA, Schmidt LD. Methane catalytic partial oxidation on autothermal Rh and Pt foam catalysts: oxidation and reforming zones, transport effects, and approach to thermodynamic equilibrium. *J Catal*. 2007;249:380–393.
31. Veser G, Schmidt LD. Ignition and extinction in the catalytic oxidation of hydrocarbons over platinum. *AIChE J*. 1996;42:1077–1087.

Manuscript received July 19, 2008, and revision received Jan. 1, 2009.